Semiconductor photocatalysts for non-oxidative coupling, dry reforming and steam reforming of methane

Katsuya Shimura [1]   and Hisao Yoshida*[2,3]

[1] Biomass Refinery Research Center, National Institute of Advanced Industrial Science and Technology (AIST), Kagamiyama 3-11-32, Higashihiroshima, Hiroshima 739-0046, Japan

[2] Department of Interdisciplinary Environment, Graduate School of Human and Environmental Studies, Kyoto University, Kyoto 606-8501, Japan

[3] Elements Strategy Initiative for Catalysts & Batteries (ESICB), Kyoto University, Kyoto 615–8520, Japan

* Corresponding author. E-mail: yoshida.hisao.2a@kyoto-u.ac.jp

Title running head: Photocatalytic Methane Conversion over Semiconductor Photocatalyst

Abstract

Methane is one of the promising alternatives of petroleum, which should be used for not only a fuel but also a resource for hydrogen and more useful chemicals as with the petroleum. However, the selective methane conversion to them is still difficult in contrast to the combustion. Three types of photocatalytic reactions for methane conversion, i.e., the photocatalytic non-oxidative coupling of methane (PNOCM: $2CH_4 \rightarrow C_2H_6 + H_2$), the photocatalytic dry reforming of methane (PDRM: $CH_4 + CO_2 \rightarrow 2CO + 2H_2$) and the photocatalytic steam reforming of methane (PSRM: $CH_4 + 2H_2O \rightarrow 4H_2 + CO_2$), can take place around room temperature or at a mild condition (ca. 473 K) using photoenergy and semiconductor photocatalyst. In the present short review, the details of each photocatalytic reaction and the design concept of the semiconductor photocatalysts for each photocatalytic methane conversion were summarized and discussed.

Keywords: Semiconductor photocatalyst, Photocatalytic non-oxidative coupling of methane, Photocatalytic dry reforming of methane, Photocatalytic steam reforming of methane

1. Introduction

Since methane is the most stable hydrocarbon molecule and thus exists not only as an abundant natural resource (e.g., natural gas, shale gas and methane hydrate) but also as a main component of biogas (biomethane) that is an important renewable resource, methane is recognized as one of the alternatives of oil resources. Although the direct combustion of methane by molecular oxygen gives us thermal or mechanical energy, we have to consider to utilize methane as not only a fuel but also a chemical raw material., i.e., it is

also important to convert methane into hydrogen and more useful chemicals as the petroleum is currently used as both fuel and chemical feedstock. Therefore, effective utilization method for the methane conversion has been widely studied. However, except for the combustion, the methane conversion usually requires much energy such as high reaction temperature, since methane is the most stable compound among hydrocarbons [1]. For instance, steam reforming of methane (SRM, $CH_4 + H_2O \rightarrow 3H_2 + CO$) using heterogeneous catalyst such as Ni or Ru has been industrially employed for the production of hydrogen or syngas from natural gas [2–4]. However, high temperature typically more than 1073 K is required for the SRM even in the presence of these established catalysts due to the positive and large Gibbs free energy change ($\Delta G^0_{298\ K} = 142$ kJ mol^{-1}) for this reaction. Furthermore, it is well-known that the side reactions such as coke formation can thermodynamically take place during methane conversion at high temperature, which results in the rapid deactivation of the catalyst. Therefore, it is very important to develop the novel process for converting methane at a milder condition, i.e., lower temperature.

Since photocatalytic reaction is driven by photoenergy without thermal activation, it can proceed even at room temperature. In addition, photocatalysts can promote not only down-hill reactions ($\Delta G < 0$) but also up-hill reactions ($\Delta G > 0$) even at low temperature, since the photoenergy compensates the increase of Gibbs free energy of the reaction system. In the photocatalytic reactions, semiconductors such as TiO_2 are typically employed as the photocatalyst. When a semiconductor photocatalyst absorbs the photoenergy more than its bandgap, photoexcitation occurs via electron transfer from the conduction band to the valence band. As a result, many holes and excited electrons are generated at the valence band and the conduction band,

respectively, both of which have high potential enough to promote many kinds of half reactions (Fig. 1a). Therefore, they can promote even difficult reactions through the oxidative and reductive half reactions. On the other hand, highly dispersed photocatalysts are another type of the heterogeneous photocatalysts, which have been mentioned as single site photocatalysts, quantum photocatalysts or local excitation photocatalysts, with a unique structures and excitation states of the active sites [5, 6]. In this type of photocatalysts, the active sites such as Ti cations are supported by insulating materials such as silica and zeolite, and the metal cation is coordinated by some oxygen anions on the surface of the support. The photoexcitation takes place at the isolated active sites, as representatively shown in Fig. 1b. It has been reported that the highly dispersed photocatalysts can promote many kinds of reactions selectively. With these photocatalysts, i.e., the semiconductors and the highly dispersed ones, some kinds of photocatalytic reactions for methane conversion could proceed around room temperature or at a mild condition, for example, the non-oxidative coupling of methane in the absence of molecular oxygen (ΔG^0_{298K} = 68.6 kJ mol^{-1}) [1, 7, 8] and the partial oxidation methane by molecular oxygen to form methanol and formaldehyde (ΔG^0_{298K} = -223 and -104 kJ mol^{-1}, respectively) [1, 9–14] and so on.

Our research group has found and developed some photocatalytic reactions, i.e., the photocatalytic non-oxidative coupling of methane (PNOCM) at room temperature, the photocatalytic dry reforming of methane (PDRM) at a mild condition (ca. 473 K), and the photocatalytic steam reforming of methane (PSRM) around room temperature over the highly dispersed photocatalysts and/or the semiconductor ones. In the present short review, we focus the semiconductor photocatalysts and discuss the design concept of

4

semiconductor photocatalysts for each photocatalytic methane conversion.

2. Photocatalytic non-oxidative coupling of methane over gallium oxide

PNOCM (Eq. 1) has been reported to proceed over several photocatalysts around room temperature under the photoirradiation with the energy enough to excite the photocatalyst in the presence of methane and in the absence of other reactive molecules.

$$2 \, CH_4 \rightarrow C_2H_6 + H_2, \quad \Delta G^0_{298 \, K} = 68.6 \, kJ \, mol^{-1} \tag{1}$$

This photocatalytic reaction was first reported with well dehydrated amorphous silica-alumina, the SiO_2-Al_2O_3 photocatalyst, in 1998 [15]. Since then, several kinds of highly dispersed photocatalysts such as TiO_2-SiO_2 photocatalyst [16], Ce/SiO_2 photocatalyst [17] and Zr/SiO_2 photocatalyst [18] were developed for this reaction. These highly dispersed photocatalysts based on silica are stable in such reductive atmosphere, i.e., in the presence of reductive gases such as methane and produced hydrogen upon photoirradiation. On the other hand, most of the semiconductor photocatalysts were unavailable for this reaction since these photocatalysts themselves could be easily photoreduced in such reductive condition; i.e., when the semiconductor photocatalysts such as TiO_2, CeO_2 and ZrO_2 were photoirradiated in the presence of methane, small amount of ethane was certainly produced but hydrogen was not obtained at all, and was consumed to reduce the semiconductors. The unique structure of the highly dispersed photocatalyst would be very important; i.e., the surrounding insulator materials such as silica would be advantageous for the durability against the photoreduction.

In order to enhance the activity of highly dispersed photocatalysts, it would be a simple idea to increase in the number of the highly dispersed active sites on the surface of support. However, the increase in the loading amount of the active metal species usually results in aggregation of these surface species and rather decreases the photocatalytic activity, which gives a limitation of the number of the active sites in this type of photocatalyst. In this strategy, further innovative method is desired to prepare such highly loaded and highly dispersed photocatalysts.

Thus, in an opposite manner, semiconductor photocatalysts having high durability against the photoreduction in the presence of methane and hydrogen have been explored. Among the examined samples, it was found that beta-type gallium oxide (β-Ga_2O_3) could promote the PNOCM with the formation of hydrogen and hydrocarbons in the stoichiometric ratio of the products around room temperature [19, 20]. Although the gallium oxide might be classified as not a semiconductor but an insulator, in this article we define the semiconductor photocatalyst to be the metal oxide that can be excited by the UV and/or visible light and can promote photocatalysis. Since gallium is not a transition metal, the Ga_2O_3 photocatalyst had a high durability against the photoreduction. Methane conversion over the β-Ga_2O_3 photocatalyst was 7 times as high as that over the Ga(0.1 mol%)/SiO_2 photocatalyst that was the highly dispersed photocatalysts, although the ethane selectivity over β-Ga_2O_3 (96%) was the same as that over Ga(0.1 mol%)/SiO_2 (Fig. 2). Furthermore, the activity of the β-Ga_2O_3 photocatalyst was comparable to that of the TiO_2-SiO_2 photocatalyst, which showed the highest activity among the highly dispersed photocatalysts that we have studied. This would originate from the higher photoabsorption efficiency and larger number of the active sites on the surface of the

6

semiconductor photocatalyst.

Increase of the reaction temperature enhanced the reaction rate for the PNOCM over the β-Ga$_2$O$_3$ photocatalyst although the successive coupling reactions and the dehydrogenation of the products also proceeded to produce the excess amount of hydrogen. For example, ethane production at 473 K was twice as large as that at 314 K (Table 1, entries 1 and 3), when the photocatalytic reaction was carried out using the closed reactor (Fig. 3a) for 3 h in the presence of methane (200 μmol) and the β-Ga$_2$O$_3$ photocatalyst powder (0.2 g). The thermal activation might contribute to desorption of products such as ethane and other hydrocarbons and/or to accelerate the migration of photoexcited electrons and holes as discussed later [21].

The β-Ga$_2$O$_3$ photocatalyst with a low surface area (2 m^2 g^{-1}) showed a higher activity than that with a higher surface area (18 m^2 g^{-1}). Further, in Fig. 2, the hydrocarbon yield increased with increasing the Ga content and reached a plateau over 2 mol % of Ga, in which Ga oxide species would form very small size of gallium oxide particles on the surface of silica. These small particles showed less activity than the bulk β-Ga$_2$O$_3$ photocatalyst (shown at 100% of Ga content). These results suggest that semiconductor photocatalyst with a larger crystallite size with fewer crystal defects would be more effective than those with a larger surface area in this photocatalytic reaction. It is generally considered that photocatalysts with a large crystallites size (i.e., high crystallinity) have few grain boundaries and crystal defects, which would act as recombination sites for the photoexcited electrons and holes, and thus facilitate the migration of these carriers. In contrast, photocatalysts with high surface area (i.e., small particle size) have many adsorption and reaction sites of reactants, and could accelerate the reaction rate. High surface area may also contribute to provide the

short migration distance for the photogenerated carriers from the inside to the surface of the bulk, which could decrease the recombination probability. We tentatively propose that in the PNOCM over the β-Ga$_2$O$_3$ photocatalyst, migration and recombination of photoexcited carriers may determine the whole reaction rate.

As for the PNOCM, although the catalyst design concept has not been completely established, the highly active photocatalyst would be summarized as follows; the semiconductor photocatalyst having a wide wavelength range of photoabsorption band, a large size of crystallites with fewer crystal defects and a high durability against photoreduction. In addition, it is better to use the photocatalyst at higher temperature than room temperature.

3. **Photocatalytic dry reforming of methane over gallium oxide**

There were only a few reports for the photocatalytic reaction between methane and carbon dioxide. For example, Tanaka and colleagues found that photoirradiation on ZrO$_2$ [22] and MgO [23] in the presence of methane and carbon dioxide allowed to produce carbon monoxide and hydrogen, where it was confirmed that carbon monoxide was produced from carbon dioxide, not from methane. Methane only took part in the formation of the active surface acetate and formate species as a reductant (hydrogen donor). Zhong et al. also reported that a Cu/CdS-TiO$_2$/SiO$_2$ photocatalyst produced acetone with high selectivity (92%) at 393 K under the irradiation of UV light [24]. However, PDRM shown in Eq. 2 had not been reported.

$$CH_4 + CO_2 \rightarrow 2CO + 2H_2, \quad \Delta G^0_{298 \text{ K}} = 170 \text{ kJ mol}^{-1} \qquad (2)$$
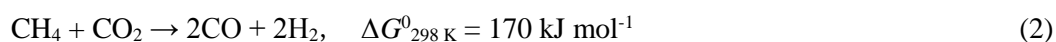
The photocatalytic reaction of methane and carbon dioxide was examined over β-Ga$_2$O$_3$ photocatalyst using

8

the closed reactor as shown in Fig. 3a [19]. When the photoirradiation was carried out at 314 K, the PNOCM dominantly proceeded and only a trace amount of carbon monoxide was formed (Table 1, entry 2). However, an increase in the reaction temperature up to 473 K enabled the formation of carbon monoxide, although formation of hydrogen and hydrocarbons (mainly ethane) was also observed (Table 1, entry 4). The stoichiometry of the products showed that both the PNOCM and the PDRM simultaneously and almost equally proceeded over the β-Ga_2O_3 photocatalyst upon photoirradiation at 473 K.

The production rate of carbon monoxide over the β-Ga_2O_3 photocatalyst through the PDRM increased with increasing the reaction temperature up to 673 K. The thermal activation energy for the formation of carbon monoxide was roughly estimated to be ca. 10 kJ mol^{-1} at 473–673 K. This value was much lower than the activation energy over this β-Ga_2O_3 sample for the thermal DRM without photoirradiation (110 kJ mol^{-1} at 773–973 K). Furthermore, carbon monoxide was not produced without photoirradiation at less than 673 K. These results suggest that the PDRM over the β-Ga_2O_3 sample should be mainly promoted by the photoenergy while the thermal energy would contribute to the mild activation steps in the whole photocatalytic reaction mechanism such as desorption of products. Since the sunlight can provide both photoenergy and thermal energy, the thermally assisted PDRM promoted at a mild temperature would be available by using solar energy. It is suggested that thermal assistance of the photocatalytic reaction would be one of the effective ways to enhance the photocatalytic activity in many other systems.

Several Ga_2O_3 photocatalysts with the different crystal phase and specific surface area were prepared by a homogeneous precipitation method, followed by calcination at various temperatures (823–1473 K) [25]. The

9

prepared Ga_2O_3 samples consisted of homogeneous granules having short rod-like morphology (300–500 nm in diameter and 1-2 μm in length). The samples calcined at 823 and 873 K consisted of α-Ga_2O_3 crystallites and those calcined at 923 K and higher temperatures consisted of β-Ga_2O_3 crystallites. The photocatalytic reaction was carried out in the presence of methane and carbon dioxide at 523 K, where the product selectivity largely depended on the surface area of the Ga_2O_3 photocatalyst. Over the photocatalysts with a low surface area, both the PNOCM and the PDRM proceeded. On the other hand, the photocatalysts with a high surface area promoted not only the PNOCM and the PDRM but also the reduction of carbon dioxide with the produced hydrogen (the reverse water-gas shift reaction; $CO_2 + H_2 \rightarrow CO + H_2O$) to enhance the selectivity to carbon monoxide. The highest selectivity of the PDRM (79%) was obtained over the catalyst calcined at 1273 K. These results demonstrated that surface structure of the photocatalyst would be one of the important factors to determine the selectivity of the Ga_2O_3 photocatalyst for the PDRM.

4. Photocatalytic steam reforming of methane over metal-loaded semiconductor photocatalysts

4.1 Outline of PSRM

Whilst photocatalytic conversion of methane with liquid water over some metal oxides (e.g. WO_3 and TiO_2) upon photoirradiation has been reported to yield methanol [26–29], there had been no photocatalytic systems reported to produce hydrogen constantly from methane with water. Our research group found that some metal-loaded semiconductor photocatalysts continuously promoted the PSRM (Eq. 3) around room temperature [30].

$$CH_4 + 2\ H_2O \rightarrow 4\ H_2 + CO_2\ , \qquad \Delta G^0_{298K} = 113\ \text{kJ mol}^{-1} \qquad\qquad (3)$$
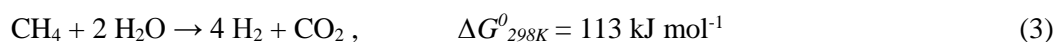
As mentioned above, when methane is consumed by complete oxidation with oxygen, we can obtain thermal or mechanical energy with an emission of carbon dioxide and water. In the PSRM, using water as an oxidant, we can obtain hydrogen in addition to carbon dioxide, where the chemical potential is increased through this reaction ($\Delta G^0_{298K} = 113$ kJ mol^{-1}). Since the increase of chemical potential originates from photoenergy, it would be able to realize solar energy conversion into hydrogen by using this photocatalytic system. The storable chemical potential of hydrogen is more useful than sunlight itself that is of low energy density and also dissipative. In this reaction carbon dioxide as one of the greenhouse gases is formed. However, since methane has much higher global warming potential than carbon dioxide, which is ca. 25 times as much as that of the same mass of carbon dioxide, conversion of methane to carbon dioxide and hydrogen should be more benefitical than releasing methane as it is into the atmosphere, which contributes to reduce the emission of greenhouse gases. From the viewpoint of carbon cycle, if the biomethane is employed, this reaction can also contribute carbon neutrality.

In the typical SRM using only thermal energy and heterogeneous catalysts, the SRM ($CH_4 + H_2O \rightarrow 3H_2 + CO$) proceeds along with the water-gas shift reaction (WGS: $CO + H_2O \rightarrow H_2 + CO_2$) to give hydrogen, carbon monoxide and carbon dioxide as the main products. Thus, the molar ratio of hydrogen to carbon monoxide depends on the reaction condition. When necessary, catalyst for the WGS is employed often as an additional process to yield more hydrogen. However, it should be noted that the PSRM can directly produce hydrogen and carbon dioxide without carbon monoxide formation very selectively, where the molar ratio of

hydrogen to carbon dioxide is usually four as shown in eq. (3).

In this reaction system, water can act as an oxidant to oxidize methane. The presence of oxidant provides high reaction rate and thus other side reactions such as PNOCM and PDRM could not proceed. Because of the high reaction rate, the reaction test of the PSRM can be carried out using the flow reactor illustrated in Fig. 3b. Typically, the photocatalyst powder (1.0 g) granulated to the size of 400–600 μm was filled up in the quartz cell ($60 \times 20 \times 1$ mm^3) [31]. The reaction was carried out upon photoirradiation with a 300 W xenon lamp from the side in the flow of the reaction gas (H_2O vapor 1.5% and CH_4 50% with Ar balance, 50 ml min^{-1}). In a standard condition, the light intensities measured in the range of 254 ± 10 and 365 ± 15 nm were ca. 14 and 60 mW cm^{-2}, respectively, and the temperature of reaction cell increased to ca. 348 K during the photoirradiation.

Several metal-loaded semiconductor photocatalysts were found to be effective for the PSRM, such as Pt-loaded TiO_2 (Pt/TiO_2) [30, 31], Pt-loaded La-doped $NaTaO_3$ (Pt/$NaTaO_3$:La) [30, 32], Pt-loaded $CaTiO_3$ (Pt/$CaTiO_3$) [33, 34], Pt-loaded Ga_2O_3 (Pt/Ga_2O_3) [21, 35, 36] and Rh-loaded $K_2Ti_6O_{13}$ (Rh/$K_2Ti_6O_{13}$) [37, 38]. Among them, the Pt/$NaTaO_3$:La photocatalyst showed the highest hydrogen production rate (1.8 μmol min^{-1}) when the photocatalytic reaction tests were carried out in the standard reaction condition mentioned above. Fig. 4 shows the time course of the production rate with the Pt(0.1 wt%)/$NaTaO_3$:La photocatalyst under the standard reaction condition as the representative [32]. After the short induction period, the hydrogen production rate became constant and it sustained without deactivation for a long period. The molar ratio of hydrogen to carbon dioxide in the outlet gas was almost constant to be four in the steady state. The formation of byproducts such as ethane and carbon monoxide was not observed. Of course, this reaction did not proceed

in the dark or without photocatalysts. The turnover frequency per the surface Pt atom of cocatalyst was estimated to be 68 h^{-1}. These facts confirmed that PSRM proceeded photocatalytically with very high selectivity. The apparent quantum yield of the PSRM system employing the Pt/NaTaO$_3$:La photocatalyst was estimated to be 30% in the range of 240–270 nm at low light intensity (2 mW cm^{-2}). This value was higher than the quantum yield of water splitting in this reaction condition employing a NiO/NaTaO$_3$:La photocatalyst [39], which is one of the best photocatalysts for water splitting. This showed that the present PSRM could produce hydrogen more efficiently than the water splitting systems. When the reaction was carried out using the Pt/NaTaO$_3$:La photocatalyst and the present reaction setup under the optimum reaction condition (CH$_4$:10%, H$_2$O:1%, light intensity at 254±10 nm: 116 mW cm^{-2}), the hydrogen production rate was 4.5 µmol min^{-1} (6.6 mL h^{-1}) and the conversion of methane and water reached to 0.6% and 11%, respectively. However, the efficiency of this system is still far from the practical use. The development of more active photocatalyst and also the improvement of photoreactor would be necessary.

4.2 Reaction mechanism of PSRM

In the PSRM over the Pt/TiO$_2$ photocatalyst, the induction period was observed more clearly and the color of the catalyst at the photoirradiated side of the reaction cell turned pale brown during the photoirradiation [31], which was suitable for the study of the reaction mechanism. It was clarified that the reaction intermediates could be described as [CH$_2$O]$_{n, ad}$, which can react with water to form products. They accumulated on the photocatalyst surface during the induction period, and interestingly, the moderate accumulation of the reaction intermediates accelerated the reaction rate. It is suggested that the hydrophobic

13

property of the surface reaction intermediates would promote the adsorption of methane. Increase of the light

intensity and the methane concentration with a moderate humidity promoted the accumulation of the reaction

intermediates on the surface and thus increased the reaction rate of the PSRM. However, it should be

important to maintain the suitable balance among the photoabsorption, molecular adsorption and the

intermediates coverage on the photocatalyst surface. The details of the reaction mechanism of each elementary

step in the PSRM are still unclear but we propose the whole mechanism as shown in Fig. 5. First, when the

photocatalyst is photoirradiated, electron and hole pairs are produced in the conduction and the valence bands,

respectively, and they migrate to the surface, i.e., to the Pt nanoparticles and the surface oxygen of the

semiconductor, respectively. Adsorbed water and methane are activated by the photoformed holes and react to

form the surface organic intermediates. Then, the reaction intermediates further react with water to produce

carbon dioxide and water. On the other hand, protons are reduced by the photoexcited electrons on the Pt

nanoparticles to form molecular hydrogen. As the result, the overall chemical equation of the PSRM in the

steady state can be described as Eq. 3.

4.3 Effect of structure and modification of photocatalysts

The photocatalytic activity for the PSRM largely depended on the crystallite size and the specific surface

area of the semiconductor photocatalyst. For example, in the PSRM over the Pt/TiO$_2$ photocatalyst, the

photocatalytic activity increased with increasing the specific surface area of the photocatalyst [31]. In the

PSRM over the Pt/NaTaO$_3$:La photocatalyst, the catalyst with the large crystallites size (low surface area)

showed higher activity than that with the small crystallite size (high surface area) [32]. In the PSRM over a

14

Pt/CaTiO$_3$ photocatalysts, the photocatalysts with the moderate surface area tended to show high catalytic

activity [34]. Then, since we noticed that the Ga$_2$O$_3$ photocatalyst could promote both water decomposition

(WD: H$_2$O→H$_2$+1/2O$_2$) and the methane decomposition (MD: CH$_4$ $\rightarrow$ 1/2xH$_2$ $+$ CH$_{4-x}$) independently, we

prepared various Pt/Ga$_2$O$_3$ photocatalysts with the different specific surface area and examined the effect of

the surface area on the photocatalytic activity in detail [35]. With increasing the surface area of the

photocatalyst, hydrogen production rate in the PSRM over Pt/Ga$_2$O$_3$ increased until it became constant (Fig.

6a), that in the WD decreased (Fig. 6b), but that in the MD increased (Fig. 6c). This suggests that the reaction

rate for the water activation would be mainly determined by the bulk process (e.g. generation, separation,

migration and recombination of electrons and holes in the bulk of semiconductor) and that for the methane

activation would be determined by the surface process (e.g. the adsorption of reactants and the surface

reactions). In the case of the PSRM, since the activation of both water and methane would be necessary, there

would be the optimum value of the specific surface area. These results indicate that photocatalyst having both

large surface area (i.e., many adsorption and reaction sites) and high crystallinity (i.e., few crystal defects)

should be ideal for the PSRM, as expected.

Addition of suitable metal ions to the semiconductor photocatalyst was an effective way to increase the

activity for the PSRM [32, 35, 36]. Table 2 shows the case of the Ga$_2$O$_3$ photocatalyst [35]. The hydrogen

production rate over Mg-doped Pt/Ga$_2$O$_3$ (Pt/Ga$_2$O$_3$:Mg) was higher than that over the bare Pt/Ga$_2$O$_3$, since

Mg ions doped in the bulk of Ga$_2$O$_3$ particles would improve the bulk property of the Ga$_2$O$_3$ photocatalyst and

contribute to the improvement of water activation. The photocatalytic activity of In-loaded Pt/Ga$_2$O$_3$

(Pt/In/Ga_2O_3) was also higher than that of Pt/Ga_2O_3, since the addition of In ions on the surface of the Ga_2O_3

particles would improve the surface property of the Ga_2O_3 photocatalyst and contribute to the improvement of

methane activation. Furthermore, the doubly modified Pt/In/Ga_2O_3:Mg photocatalyst showed higher activity

than the Pt/Ga_2O_3:Mg and Pt/In/Ga_2O_3 samples, since both modifications, i.e., Mg-doping in the bulk and

In-loading on the surface, would contribute to the enhancement of the activity independently at the same time.

In the PSRM over the Pt/$NaTaO_3$:La photocatalyst, the photocatalytic activity was largely influenced by the

Pt-loading method [32]. Fig. 7 shows the time course of hydrogen production rate in the PSRM over three

Pt/$NaTaO_3$:La photocatalysts prepared by different Pt-loading method, i.e., (a) by a photodeposition method,

(b) by the photodeposition method followed by calcination and reduction at 773 K, and (c) by an impregnation

method followed by calcination and hydrogen reduction at 773 K. It is believed that the photodeposition

method could deposit metal nanoparticles selectively on the surface reductive sites by utilizing the

photocatalytic property and thus could provide efficient metal-loaded photocatalysts. However, the activity of

the Pt/$NaTaO_3$:La photocatalyst prepared by the photodepoision method drastically decreased with time

during the reaction (Fig. 7a). TEM observation revealed that the aggregation of Pt nano-particle occurred

during the photocatalytic reaction. On the other hand, the activity of thermally treated samples did not

deactivate during the reaction (Fig. 7b and 7c). This is because the thermal treatment would improve the

metal-semiconductor junction between the Pt nanoparticles and the surface of the $NaTaO_3$:La semiconductor,

which would be important for both the activity and the stability. The highest activity was obtained over the

catalyst prepared by impregnation method followed by calcination and hydrogen reduction at 773 K (Fig. 7c).

16

These results clearly show that the stability of the metal-semiconductor junction should be one of the important factors to determine the performance of the semiconductor photocatalyst.

The activity of the $K_2Ti_6O_{13}$ photocatalyst largely depended on the metal cocatalyst and its loading method [37, 38]. Although loading Pt cocatalyst largely increased the photocatalytic activity of the $K_2Ti_6O_{13}$ photocatalyst, it induced a formation of carbon monoxide as the minor byproduct and the small deactivation of the photocatalyst with time. On the other hand, a Rh-loaded $K_2Ti_6O_{13}$ sample prepared by the photodeposition method in the presence of dissolved oxygen showed two times higher activity than the Pt-loaded one did, with a high selectivity without deactivation. Analysis with XAFS and TEM revealed that, the Rh cocatalyst in the highly active $Rh/K_2Ti_6O_{13}$ photocatalyst existed as a mixture of small metallic rhodium and large rhodium oxide particles. The photocatalytic activity tests for hydrogen evolution and oxygen evolution from each aqueous solution of sacrificial reagent (methanol and silver nitrate, respectively) also clarified that the metallic rhodium particles and the rhodium oxide particles could function as cocatalysts preferably for reduction and oxidation, respectively. Therefore, we proposed that the bifunctional Rh cocatalyst on the $K_2Ti_6O_{13}$ photocatalyst cooperatively promoted the reductive and oxidative reactions, respectively, to increase the entire photocatalytic activity for the PSRM (Fig. 8).

4.4 Effect of thermal activation

Thermal acceleration of the photocatalytic reaction rate was confirmed for the PSRM also [21, 32, 36]. Fig. 9 shows the time course of the hydrogen production rate in the PSRM over Pt/Ga_2O_3 at stepwise-increasing temperature and the corresponding Arrhenius plot [21], where the hydrogen production rate increased before it

17

became constant. In the lower temperature range between 318 and 334 K, the Arrhenius plot showed a straight line and the thermal activation energy (E_a) was calculated to be 5.4 kJ mol^{-1} in this case. The E_a value varied with the structure of Ga_2O_3, the loading of metal cocatalyst and the reaction condition. However, the E_a values were typically lower than ca. 20 kJ mol^{-1}, which is too small to promote usual chemical reactions or catalytic reactions. Therefore, it was suggested that the thermal energy for the PSRM would contribute to the mild activation steps only. This means that the photoenergy surely gives the main driving force. Several detailed experiments suggested that the thermal energy would contribute to the migration of photoexcited carriers through the conduction/valence bands in the bulk of the Ga_2O_3 particles as well as electron transfer at the metal-semiconductor junction between the Ga_2O_3 particles and the metal cocatalyst, as shown in Fig. 10. In the low intensity of the incident light, or in the photocatalysts consisting of small crystallites having low crystallinity with many trap sites, large thermal activation energy was required to realize the smooth migration of photoexcited carriers. In the samples loaded with small metal nano-particles, the additional thermal energy largely enhanced the photocatalytic activity since it would help the electrons to transfer from the conduction band to the metal cocatalysts beyond the high Schottky barrier. It is generally expected that studying thermal activation energy in photocatalysis would be useful to know the influence of defects and metal-semiconductor junction of semiconductor photocatalysts.

5. Conclusion

In a photocatalytic system, the use of photoenergy with a photocatalyst can promote the thermodynamically

unfavorable reaction under the mild reaction condition even at room temperature. It should be also noted that photocatalysis can convert the photoenergy (e.g. solar energy) into the storable chemical products of high potential (e.g. hydrogen). Our research group found three kinds of photocatalytic reactions concerning methane conversion, i.e., the photocatalytic non-oxidative coupling of methane (PNOCM), the photocatalytic dry reforming of methane (PDRM) and the photocatalytic steam reforming of methane (PSRM). These photocatalytic reactions could proceed at a mild condition (less than 473 K) by using semiconductor photocatalysts. We have also obtained some knowledge about the mechanism of each photocatalytic reaction and the catalyst design concept to some extent so far.

For the PNOCM and the PDRM, high photocatalytic activity was obtained over the photocatalysts having the high durability against the photoreduction by methane and hydrogen. It was also clarified that the additional thermal energy could largely enhance the reaction rate. As a semiconductor photocatalyst showing the activity for these reactions, we have discovered the Ga_2O_3 photocatalyst. However, the efficiency of these photocatalytic systems using Ga_2O_3 photocatalyst is not enough for practical use. Further studies must be carried out in order to improve the efficiency of these photocatalytic systems, such as the exploration of other semiconductor materials, the precise structure control of semiconductor photocatalyst and the development of effective cocatalyst and additives, as well as improvements of photoreactor.

On the other hand, for the PSRM, we found several active photocatalysts. We also obtained some guidelines for catalyst design as follows: (1) It is very important to control the surface hydrophobic or hydrophilic property of the photocatalyst, since the surface property largely influences the adsorption amount of reactants

and the concentration of surface organic intermediate. (2) Photocatalysts with high surface area and few crystal defects show high catalytic activity. (3) The improvement of the processes in the bulk of semiconductor promotes the water activation, while the surface modification develops the methane activation. (4) Not only the kind of metal cocatalyst and its loading method but also the stability of the metal-semiconductor junction influences the photocatalytic activity and durability. (5) Cooperation of two kinds of cocatalysts for the oxidation and reduction enhances the photocatalytic activity. (6) Thermal activation also can assist the PSRM in some cases.

We hope that further developed systems based on these photocatalytic systems will contribute to utilize methane that can be obtained from underground and biogas, in the near future.

References

1. Yuliati L, Yoshida H (2008) Chem. Soc. Rev. 37:1592

2. Rostrup-Nielsen JR (1993) Catal. Today 18:305

3. Peña MA, Gómez JP, Fierro JLG (1996) Appl. Catal. A 144:7

4. Armor JN Appl. Catal. A (1999) 176:159

5. Yoshida H, (2003) Curr. Opin. Solid State Mater. Sci. 7:435

6. Yoshida H, (2005) Catal. Surv. Asia 9:1

7. Li L, Li GD, Yan C, Mu XY, Pan XL, Zou XX, Wang KX, Chen JS (2011) Angew. Chem. Int. Ed. 50:8299.

8. Li L, Cai YY, Li GD, Mu XY, Wang KX, Chen JS (2012) Angew. Chem. Int. Ed. 51:4702

9. Wada K, Yamada H, Watanabe Y, Mitsudo T (1998) J. Chem. Soc., Faraday Trans. 94:1771

10. López HH, Martínez A (2002) Catal. Lett. 83:37

11. Ward MD, Brazdil JF, Mehandru SP, Anderson AB (1987) J. Phys. Chem. 91:6515

12. Wada K, Yoshida K, Watanabe Y, (1995) J. Chem. Soc., Faraday Trans. 91:1647

13. Sastre F, Fornés V, Corma A, García H (2011) J. Am. Chem. Soc. 133:17257

14. Sastre F, Fornés V, Corma A, García H (2012) Chem. Eur. J. 18:1820

15. Kato Y, Yoshida H, Hattori T (1998) Chem. Commun. 2389

16. Yuliati L, Itoh H, Yoshida H (2007) Stud. Surf. Sci. Catal. 172:457

17. Yuliati L, Hamajima T, Hattori T, Yoshida H (2008) J. Phys. Chem. C 112:7223

18. Yoshida H, Chaskar MG, Kato Y, Hattori T (2003) J. Photochem. Photobio. A 160:47

19. Yuliati L, Itoh H, Yoshida H (2008) Chem. Phys. Lett. 452:178

20. Yuliati L, Hattori T, Itoh H, Yoshida H (2008) J. Catal. 257:396

21. Shimura K, Maeda K, Yoshida H, (2011) J. Phys. Chem. C 115:9041

22. Kohno Y, Tanaka T, Funabiki T, Yoshida S (2000) Phys. Chem. Chem. Phys. 2:5302

23. Teramura K, Tanaka T, Ishikawa H, Kohno Y, Funabiki T (2004) J. Phys. Chem. B108:346

24. Shi D, Feng Y, Zhong S (2004) Catal. Today 98:505

25. Yoshida H, Maeda K (2010) Stud. Surf. Sci. Catal. 175:351

26. Taylor CE (2003) Catal. Today 84:9

27. Gondal MA, Hameed A, Suwaiyan A (2003) Appl. Catal. A 243:165

28. Gondal MA, Hameed A, Yamani ZH, Arfaj A (2004) Chem. Phys. Lett. 392:372

29. Shimura K, Yoshida H (2011) Energy Environ. Sci. 4:2467

30. Yoshida H, Kato S, Hirao K, Nishimoto J, Hattori T (2007) Chem. Lett. 36:430

31. Yoshida H, Hirao K, Nishimoto J, Shimura K, Kato S, Itoh H, Hattori T (2008) J. Phys. Chem. C 112:5542

32. Shimura K, Kato S, Yoshida T, Itoh H, Hattori T, Yoshida H (2010) J. Phys. Chem. C 114:3493

33. Shimura K, Yoshida H (2010) Energy Environ. Sci. 3:615

34. Shimura K, Miyanaga H, Yoshida H (2010) Stud. Surf. Sci. Catal. 175:85

35. Shimura K., Yoshida T, Yoshida H (2010) J. Phys. Chem. C 114:11466

36. Shimura K, Yoshida H, (2012) Phys. Chem. Chem. Phys. 14:2678

37. Shimura K, Kawai H, Yoshida T, Yoshida H (2011) Chem. Commun. 47:8958

38. Shimura K, Kawai H, Yoshida T, Yoshida H (2012) ACS Catal. 2:2126

39. Kato H, Asakura K, Kudo A, (2003) J. Am. Chem. Soc. 125:3082
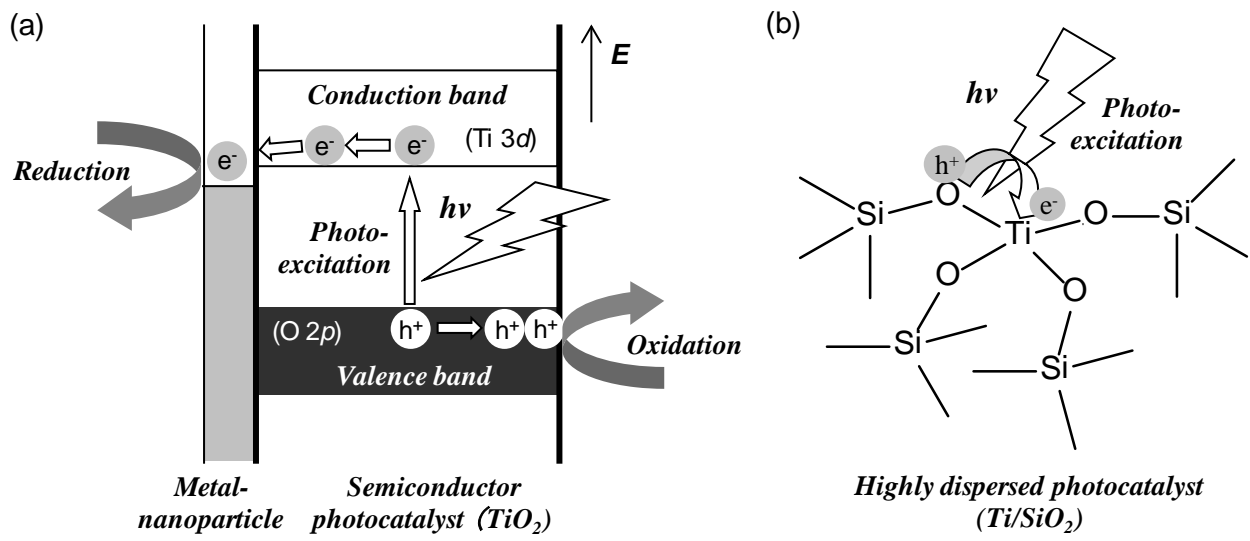
Figure captions

Fig. 1 Photoexcitation of (a) semiconductor photocatalyst (TiO_2) and (b) highly dispersed photocatalyst (Ti/SiO_2).

Fig. 2 Dependences of (a) hydrocarbon yield and (b) ethane selectivity on the Ga content of silica-supported gallium oxide samples. Ga content of 100 shows the β-Ga_2O_3 sample. Data were from [1].

Fig. 3 Schematic drawing of the photoreactors used in the present study; (a) closed reactor and (b) flow reactor.

Fig. 4 Time course of the production rate of H_2 and CO_2 on the Pt(0.1 wt%)/$NaTaO_3$:La photocatalyst, and that of molar ratio of the produced H_2 to CO_2 (H_2/CO_2) under the standard reaction condition (Catalyst: 1.0 g, CH_4: 50%, H_2O vapor: 1.5%, Flow rate: 50 ml min^{-1}, Light intensity at 254 ±10 nm: 14 mW cm^{-2}). Data were from [32].

Fig. 5 The proposed reaction mechanism for the PSRM over Pt/TiO_2 photocatalyst.

Fig. 6 Effect of the BET specific surface area of the β-Ga_2O_3 samples on the hydrogen production rate (a) in the flow of both water vapor and methane (the PSRM), (b) in the flow of water vapor (the WD) and (c) in the flow of methane (the MD). Data were from [35].

Fig. 7 Time course of the H_2 production rate on the Pt/$NaTaO_3$:La samples, on which Pt was loaded (a) by photodeposition method, (b) by photodeposition method followed by calcination and reduction at 773 K, and (c) by impregnation method followed by calcination and H_2 reduction at 773 K. Data were from [32].

Fig. 8 The proposed mechanism in the PSRM over the Rh/Rh_2O_3/$K_2Ti_6O_{13}$ photocatalyst prepared by the

oxidative photodeposition method.

Fig. 9 (A) Time course of the hydrogen production rate (V_{H2}) in the PSRM over the Pt(0.07 wt%)/Ga$_2$O$_3$

photocatalyst at stepwise-increasing temperature and (B) the corresponding Arrhenius plot. Data were from

[21].

Fig. 10 The proposed thermal activation mechanism in the PSRM over Pt/Ga$_2$O$_3$ photocatalyst.

Table 1 Results of the PNOCM and PDRM over the β-Ga_2O_3 photocatalyst[a]

Entry	Reaction temperature / K	Reactants / μmol		Products / μmol				H_2 experimental / H_2 expected
		CH_4	CO_2	C_2H_6	C_2-C_4	CO	H_2	
1	314	200	0	0.51	0.07	0	0.74	1.1
2	314	200	200	0.44	0.07	trace	0.53	0.9
3	473	200	0	1.02	0.26	0	2.41	1.5
4	473	200	200	1.04	0.29	1.08	2.48	0.9

[a] Data from ref. 19. Catalyst: 0.2 g. Irradiation time: 3 h. Light intensity: 9 mW/cm^2 in the rage of 254±10 nm.

Table 2 Loading effect of metal ions on the photocatalytic activity of the Pt/Ga_2O_3 samples for the PSRM [a]

Photocatalyst	Mg-doping / mol%	In-loading / mol%	H_2 production rate / μmol min^{-1}
Pt/Ga_2O_3	0	0	0.41
Pt/Ga_2O_3:Mg	1	0	0.55
Pt/In/Ga_2O_3	0	0.05	0.48
Pt/In/Ga_2O_3:Mg	1	0.05	0.65

[a] Data from ref. 35. Pt-loading amount: 0.01 wt%.

Fig. 1 Photoexcitation of (a) semiconductor photocatalyst (TiO$_2$) and (b) highly dispersed photocatalyst (Ti/SiO$_2$).

Fig. 2 Dependences of (a) hydrocarbon yield and (b) ethane selectivity on the Ga content of silica-supported

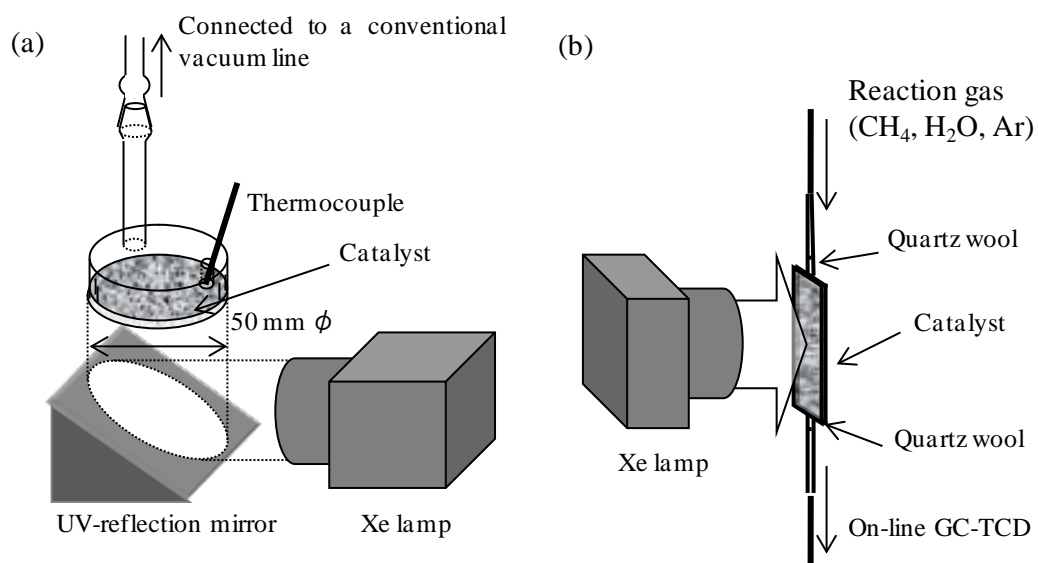gallium oxide samples. Ga content of 100 shows the β-Ga_2O_3 sample. Data were from [1].

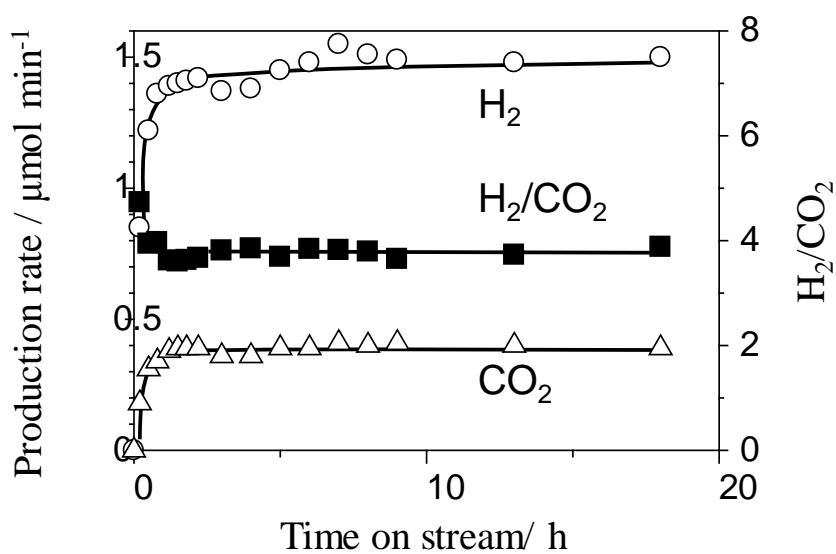**Fig. 3** Schematic drawing of the photoreactors used in the present study; (a) closed reactor and (b) flow

reactor.

Fig. 4 Time course of the production rate of H_2 and CO_2 on the Pt/(0.1 wt%)$NaTaO_3$:La photocatalyst, and that of molar ratio of the produced H_2 to CO_2 (H_2/CO_2) under the standard reaction condition (Catalyst: 1.0 g, CH_4: 50%, H_2O vapor: 1.5%, Flow rate: 50 ml min^{-1}, Light intensity at 254 ±10 nm: 14 mW cm^{-2}). Data was from [32].

Fig. 5 The proposed reaction mechanism for the PSRM over Pt/TiO$_2$ photocatalyst.

Fig. 6 Effect of the BET specific surface area of the β-Ga_2O_3 samples on the hydrogen production rate (a) in the flow of both water vapor and methane (the PSRM), (b) in the flow of water vapor (the WD) and (c) in the flow of methane (the MD). Data were from [35].
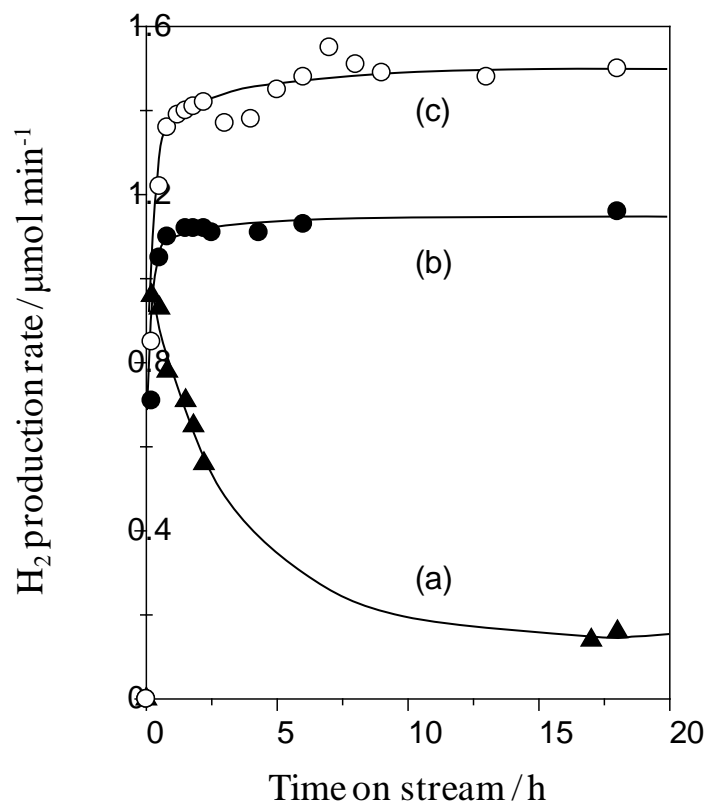
Fig. 7 Time course of the H_2 production rate on the Pt/NaTaO$_3$:La samples, on which Pt was loaded (a) by

photodeposition method, (b) by photodeposition method followed by calcination and reduction at 773 K, and

(c) by impregnation method followed by calcination and H_2 reduction at 773 K. Data were from [32].
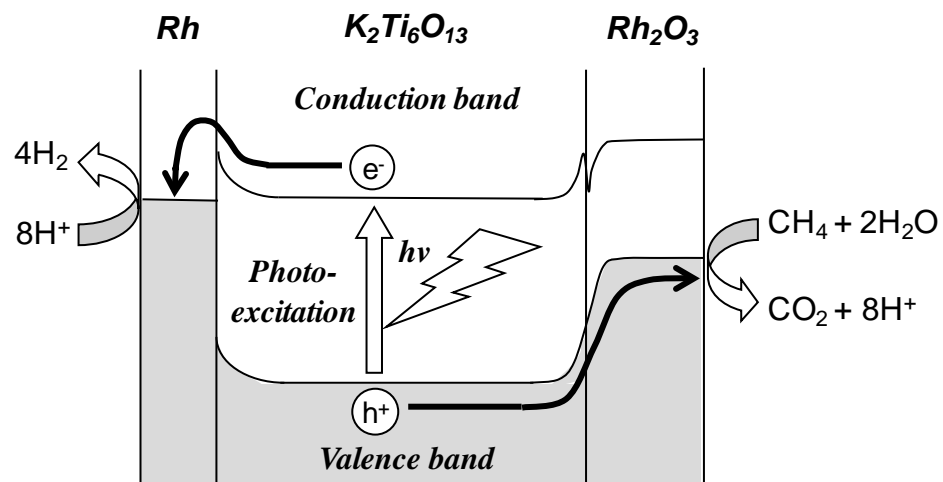
Fig. 8 The proposed mechanism in the PSRM over the Rh/Rh$_2$O$_3$/K$_2$Ti$_6$O$_{13}$ photocatalyst prepared by the
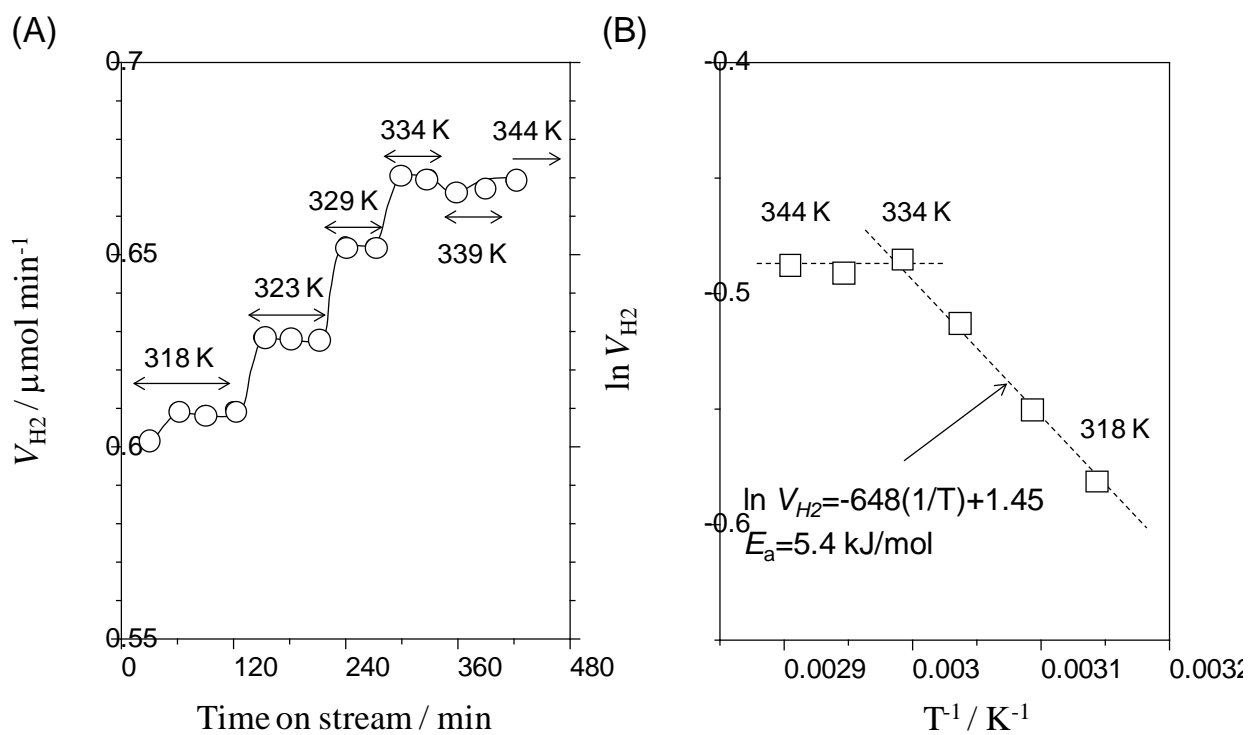
oxidative photodeposition method.

Fig. 9 (A) Time course of the hydrogen production rate (V_{H2}) in the PSRM over the Pt(0.07 wt%)/Ga_2O_3 photocatalyst at stepwise-increasing temperature and (B) the corresponding Arrhenius plot. Data were from [21].
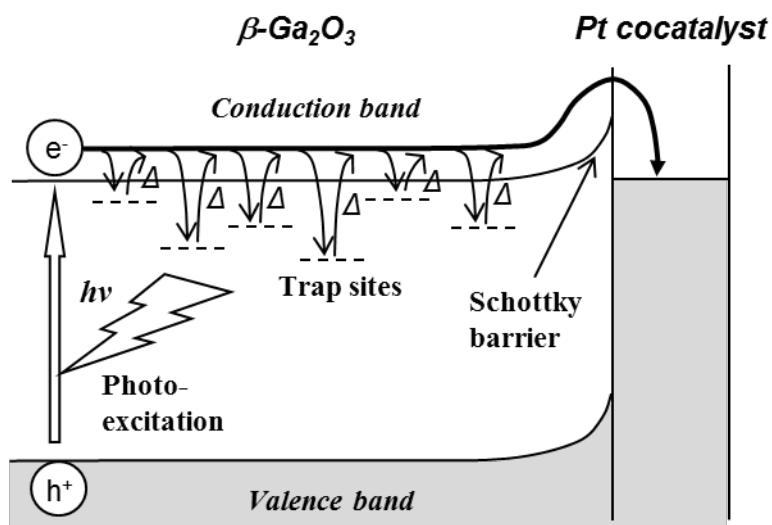
Fig. 10 The proposed thermal activation mechanism in the PSRM over Pt/Ga$_2$O$_3$ photocatalyst.